ACS APPLIED NANO MATERIALS

www.acsanm.org Article

Highly Efficient Dopamine Sensing with a Carbon Nanotube-Encapsulated Metal Chalcogenide Nanostructure

Harish Singh, Jiandong Wu, Kurt A. L. Lagemann, and Manashi Nath*

Cite This: ACS Appl. Nano Mater. 2024, 7, 4814−4823 Read Online

ACCESS | Metrics & More | Article Recommendations | Supporting Information

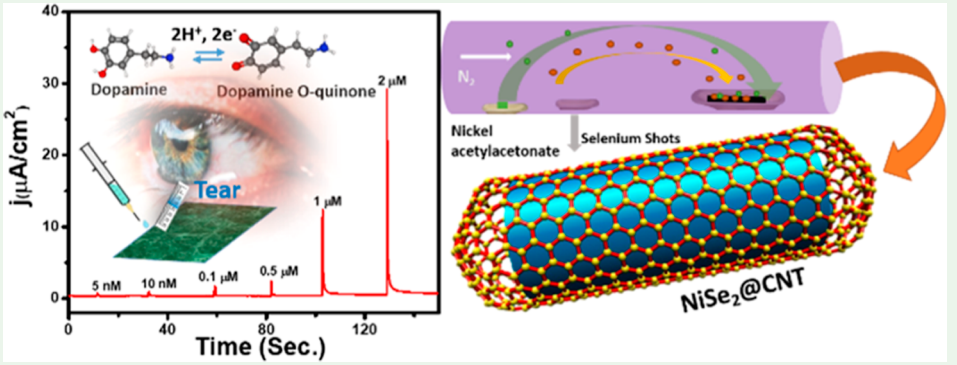

ABSTRACT: Carbon nanotube-encapsulated nickel selenide composite nanostructures were used as nonenzymatic electrochemical sensors for dopamine detection. These composite nanostructures were synthesized through a simple, one-step, and environmentally friendly chemical vapor deposition method, wherein the CNTs were formed in situ from pyrolysis of a carbon-rich metallo-organic precursor. The composition and morphology of these hybrid $NiSe_2$-filled carbon nanostructures were confirmed by powder X-ray diffraction, Raman, X-ray photoelectron spectroscopy, and high-resolution transmission electron microscopy images. Electrochemical tests demonstrated that the as-synthesized hybrid nanostructures exhibited outstanding electrocatalytic performance toward dopamine oxidation, with a high sensitivity of 19.62 $\mu A\ \mu M^{-1}\ cm^{-2}$, low detection limit, broad linear range of 5 nM−640 μM, and high selectivity. The synergistic effects of enhanced electrochemical activity of nickel selenide along with the enhanced conductivity of carbon nanotubes led to the high electrocatalytic efficiency for these nanostructured composites. The high sensitivity and selectivity of this nanostructured composite could be exploited to develop simple, selective, and sensitive electrochemical sensors to detect and quantify dopamine in human tear samples with high reliability. This nanotube-encapsulated sensor, hence, paves the way for discoveries in the development of dopamine sensors with low cost and high stability, which can be used for noninvasive dopamine detection in peripheral bodily fluids.

KEYWORDS: *dopamine sensor, metal chalcogenide nanostructures, carbon nanotube composites, nonenzymatic biosensor, dopamine oxidation*

INTRODUCTION

Dopamine (DA) is one of the most important neurotransmitters in the human body, which has been linked to critical functions of the central nervous system and regulates hormonal activities. Imbalance in DA concentrations has been linked to various neurodegenerative disorders including schizophrenia, Parkinson's, and psychosis, where low and fluctuating levels of DA are indicative of the rapid progression of these diseases.[1] High levels of DA, on the other hand, indicate cardiotoxicity and result in a faster heart rate, hypertension, and eventually heart failure.[2] It has been known that DA is intimately connected to the brain's reward system.[2] In addition to the fact that DA is a vital neurotransmitter, the use of illegal drugs or substance abuse such as heroin, cocaine, nicotine, and alcohol blocks the DA transport, which inhibits the reuptake of DA and eventually decreases the levels of DA, increasing the risk of depression.[3] Based on its implication in physical and mental well-being, detection of DA levels in the body has become extremely important. Also, it has become important to understand the interplay between various biomolecules and DA levels and the condition under which the DA level fluctuations are triggered in real time. Hence, development of continuous health

Received: November 13, 2023
Revised: February 8, 2024
Accepted: February 9, 2024
Published: February 27, 2024

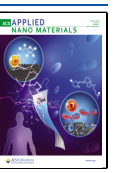

Scheme 1. (a) Oxidation scheme of DA through $1e^-$ and $2e^-$ pathways; (b) Synthesis scheme of the $NiSe_2$@CNT composite electrode

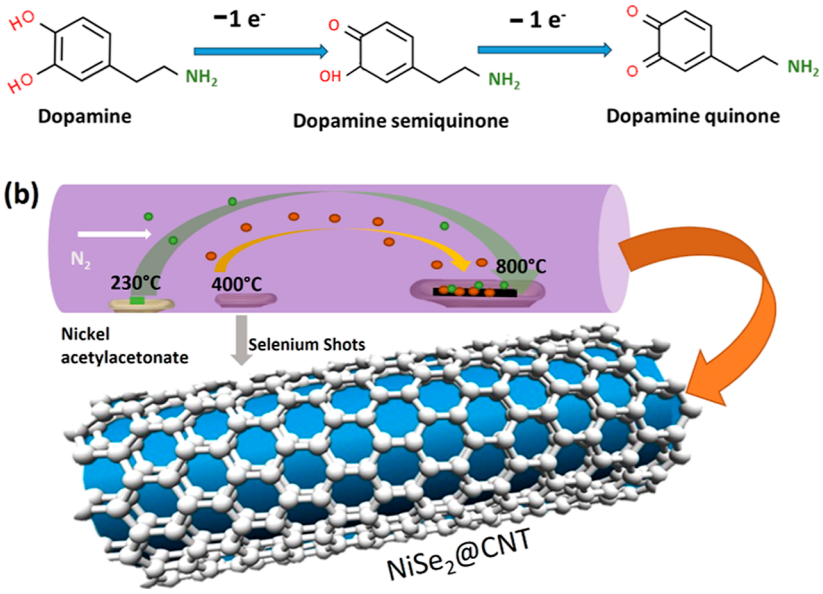

monitoring systems that can detect the level of DA continuously and its fluctuations in real time has become critical. However, the critical component for such sensors is the development of a high-sensitivity, reusable, point-of-care sensing module with long-term operational stability. One of the major challenges of detecting neurochemicals under physiological conditions is due to their low levels in various peripheral biological fluids, which makes it difficult to monitor them under stationary conditions or during medical treatments.

For the selective determination of different levels of neurotransmitters, a broad range of instrumental techniques have been used. Spectral photometry,[4] liquid chromatography,[5] and chemiluminescence[6] array are few examples among them. However, most of these reported methods suffer from many disadvantages, including but not limited to high prices and sample pretreatment criteria. Among various detection techniques, electrochemical methods are often used to detect the levels of DA.[7,8] Under physiological conditions, the $2e^-/2H^+$ redox reactions of DA forms the basis of electrochemical detection (Scheme 1a), wherein, the amount of DA in the analyte can be estimated from the oxidation current. However, the close proximity of the DA oxidation potential (E_{ox}) to that of other biomolecules found in the central nervous system presents a crucial challenge. Among these, ascorbic acid (AA), which has an oxidation potential very close to that of DA, is the main interferent species because of its abundance in serum samples where it is present in a much higher concentration compared to DA.[9] Furthermore, DA exists in a cationic form, whereas AA exists in an anionic form.

The novelty of nonenzymatic electrochemical sensors is their direct detection method, which leads to higher sensitivity and low limit of detection.[10−13] However, to achieve such high-performance metrics, the use of an electrode modified with an electrocatalyst is critical. The electrocatalyst composition optimizes the electron transfer kinetics between the analyte−electrode interface, leading to selectivity in analyte detection, while the electrode−electrocatalyst composite is expected to facilitate charge transfer and increase sensitivity of the sensor. Several nanomaterials, including metal oxides, metal selenides, carbon nanoparticles and their hybrids, have been used successively as electrocatalysts for nonenzymatic electrochemical DA and other biomolecule sensing.[7,14−17] Among the various composite-based nanomaterials (Fe, Bi, Au, Cu, Co, Ni), Ni-based hydrides were considered to be an interesting material owing to their biocompatibility, redox activity, and high electroactive surface area.[14,16,18,19]

Recently, there has been an increase in the application of transition-metal chalcogenides as electrocatalysts owing to their high electrical conductivity and enriched redox chemistry.[20,21] Examples of such transition-metal chalcogenides include molybdenum selenide ($MoSe_2$), iron selenide ($FeSe_2$), nickel selenide (NiS_2), bismuth selenide (Bi_2Se_3), and copper selenide (CuSe and Cu_2Se), which have been used as sensors.[7,8,15,22−24] Over the past few years, nickel and other transition-metal-based chalcogenides have been synthesized and explored for various electrochemical and electrocatalytic applications, including batteries,[25] carbon dioxide reduction,[26−28] oxygen evolution reaction,[29−31] hydrogen evolution reaction,[29,32] as supercapacitors,[33,34] and as solar cells.[35,36] However, the use of nickel-selenide-based compositions in electrochemical sensors is still rare.

Apart from catalyst composition, the enhanced conductivity of the composite is also critical for high sensitivity. Hence, various conductive additives, including carbon nanotubes and other nanostructures, have been used to enhance electrical conductivity and charge transport within the catalyst composite. On account of their low cost, electrical conductivity, and good corrosion resistance in a wide range of electrolytes, carbon-based nanomaterials have been widely used as electrochemical sensors.[37,38] In particular, the growth of electrocatalytic nanoparticles on the carbon-based substrates has improved electrochemical performance. However, despite having a high surface to volume ratio, CNTs are less sensitive to electro-oxidizing specific biomolecules such as DA because of the lack of catalytically active sites, requiring the use of metal nanocatalysts.[39] Hence, composite materials have been investigated for electrode modification to evaluate potential

https://doi.org/10.1021/acsanm.3c05422
ACS Appl. Nano Mater. 2024, 7, 4814−4823

synergistic effects in order to improve sensor performance such as long-term stability and selectivity. Herein, the electrocatalytic activity of carbon nanotubes filled with nickel selenide ($NiSe_2$@CNT) has been reported for the first time for effective sensing of DA. $NiSe_2$@CNT was synthesized by an innovative CVD technique using a metallo-organic molecular precursor that led to in-situ formation of multiwalled carbon nanotubes. The electrocatalytic activity for DA oxidation was studied using cyclic voltammetry (CV), chronoamperometry (CA), and differential pulse voltammetry (DPV) methods. In addition, due to their high electrical conductivity the CNTs can also facilitate electron transfer in electrochemical redox reactions, which has a synergistic effect on metal/metal chalcogenide catalytic properties.[40,41] Additionally, this electrocatalyst shows remarkable long-term stability, reproducibility, reusability, as well as a high degree of selectivity for DA oxidation in the presence of interfering molecules.

EXPERIMENTAL SECTION

Materials. L-ascorbic acid (L-AA) (99%), uric acid (UA) (99%), and serotonin hydrochloride (SA) (98%) were obtained from Alfa Aesar and were used as received. Dextrose (98%), dopamine hydrochloride, 99%, sodium chloride (99%), potassium chloride (99%), and hydrogen peroxide 35 wt % were obtained from Fisher Scientific. DA solutions were prepared by dissolving dopamine hydrochloride in a 0.1 M phosphate buffer solution (PBS). Deionized water was used to prepare all solutions. Nickel(II) bis-(acetylacetonate) ($C_{10}H_{14}NiO_4$) (96%), referred to as Ni(acac)$_2$ henceforth, and selenium shots (1−3 mm, amorphous, 99.999%) were obtained from Fisher Scientific.

$NiSe_2$@CNT Synthesis. The $NiSe_2$ nanostructure wrapped with carbon nanotubes ($NiSe_2$@CNT) was synthesized via CVD reaction carried out in a horizontal tube furnace at 800 °C under a flow of N_2 as a carrier gas (140 sccm) using sublimable Ni-acetylacetonate and Se shots as precursors. Graphite foils were used as the substrate for growth, which was kept at the central zone of the horizontal furnace at 800 °C (Scheme 1b). The reaction unit was held in a continuous N_2 flow of 140 sccm with the help of a mass flow controller. Both nickel(II) acetylacetonate and Se sublime at moderately low temperatures and were strategically located in the reaction tube so that the temperature at the precursors reached above its sublimation temperature when the central zone of the furnace was at 800 °C. Ni(acac)$_2$ and Se was originally placed outside of the heating area by moving the ceramic liner toward the extreme left. When the central zone of the furnace reached 800 °C, the ceramic liner was pulled to the right such that Se shots were located at 400 °C while Ni(acac)$_2$ was held at 230 °C. The reaction temperature was maintained at 800 °C for 30 min, and then the furnace was cooled down at 5 °C min^{-1}. After the reaction, a grayish deposition was observed on the graphite foil, which was further investigated through microscopy and structural characterization.

Characterization. The product without any further purification was characterized by powder X-ray diffraction (PXRD) with a Philips X-Pert using CuKα (1.5418 Å) radiation. As the product formed a very thin layer on the graphite foil, pxrd was collected in thin-film geometry at grazing angles (GI mode and Göbel mirrors). As-synthesized $NiSe_2$@CNT was characterized by Tecnai F20 in order to obtain high-resolution TEM (HRTEM) images. The Raman spectra of the prepared sample were acquired using a HORIBA Jobin-Yvon LabRam ARAMIS Raman spectrometer, which was equipped with a charge-coupled device detector. Each spectrum was generated by exciting the sample using the Argon ion laser with a wavelength of 532 nm and a maximum continuous-wave power of 75 mW. X-ray photoelectron spectroscopy (XPS) measurements were performed using a KRATOS AXIS 165 X-ray photoelectron spectrometer with a monochromatic Al X-ray source. The XPS examinations were carried out on the pristine catalyst surface without any sputtering. The C 1s signal at 284.5 eV served as the reference for the correction of all XPS binding energies.[42]

Electrocatalytic DA Analysis. All electrochemical research was conducted with an IviumStat potentiostat. The electrochemical experiments were performed in a three-electrode cell system with a graphite rod as the counter electrode, Ag|AgCl (KCl-saturated) as the reference electrode, and the 0.015 mm thin $NiSe_2$@CNT-loaded graphite foil substrate as the working electrode. The analysis for DA detection was conducted in an electrolyte solution of PBS with a pH of 7.0. The electrolyte solution was prepared to contain a precisely known concentration DA, ranging from 1 to 640 μM.

In this study, a 0.1 M PBS was prepared by dissolving 0.1 M dipotassium phosphate (K_2HPO_4) and potassium phosphate monobasic (KH_2PO_4). Initially, the salts were individually dissolved in distilled water with continuous stirring until complete dissolution was achieved. Subsequently, the solutions were combined and thoroughly stirred. The pH of the resulting buffer solution was measured by using a pH meter. To attain a pH of 7, incremental adjustments were made by adding small quantities of either K_2HPO_4 or KH_2PO_4, as required.

Electrochemical Method for Tear Analysis. Schirmer strips have been effectively utilized to assess DA levels in humans by indirect tear collection. Tear retrieval techniques involving Schirmer strips are easy to use and secure and yield a sufficient quantity of tear fluid suitable for a wide spectrum of bioanalytical applications. In our research, we employed this method for tear collection to enable the electrochemical detection of DA molecules. Tear samples from healthy individuals were used to determine the DA levels. Collection with Schirmer strips was accomplished by inserting the strips into the lower conjunctival fornix until the strip became moist at the 25 mm mark. The strips were bent, inserted at a center position, and utilized with closed eyes for a few minutes. After the collection of tears, the Schirmer strips were immersed in 0.1 M PBS and centrifuged to remove any impurities from the tears. Following 15 min of centrifugation, the supernatant from each sample vial was transferred to a 0.2 μL spin filter and centrifuged for another 15 min at 10,000 rpm to remove any remaining contaminants. 50 μL of dissolved tears in 0.1 M PBS was taken and used for electrochemical detection of DA using the CA technique. To preserve them until further use, tear samples and strips were stored at a temperature of −80 °C.

HPLC-MS/MS Method. A Shimadzu (Columbia, MD, USA) Prominence UFLC system coupled to a 4000Q TRAP tandem mass spectrometer system (AB SCIEX, Concord, ON, CA) was used for HPLC analysis. A HydroRP column (4 μm, 250 × 2 mm) purchased from Phenomenex (Torrance, CA, USA) was employed. HPLC was performed with the binary flow at a rate of 0.3 mL/min with mobile phase **A** consisting of 0.01% formic acid in ultrapure water and mobile phase **B** consisting of 0.01% formic acid in acetonitrile (ACN). The column oven temperature was set at 40 °C. After injection of 20 μL of the sample, the method began with 100% **A** for 1.0 min, followed by a linear gradient of 0−100% **B** from 1.0 to 7.5 min. After holding at 100% **B** from 7.5 to 8.0 min, the mobile phase was changed back to 100% **A** from 8.0 to 9.0 min, followed by a 5 min re-equilibration with 100% **A** before the next injection. Positive electrospray ionization mode and multiple reaction monitoring (MRM) were used for the quantification analysis. Two mass transitions were monitored for DA (Table S1). The ion source temperature was set to 550 °C. The ion spray voltage was set to 4500 V. The curtain gas was set to 15 psi, and the ion source gases (GS1 and GS2) were at 35 and 45 psi, respectively.

RESULTS AND DISCUSSION

Structure and Morphologies of Nanocomposites. Nickel selenide wrapped with CNTs on graphite foils were made by catalytic chemical vapor deposition. The choice of the nickel precursor Ni(acac)$_2$, containing two acetylacetonate ligands, played a pivotal role in facilitating CNT formation by providing an in situ source for generating carbon-rich vapors. Because Ni is also catalytic toward the growth of carbon nanotubes through CVD of hydrocarbon, the unique

https://doi.org/10.1021/acsanm.3c05422
ACS Appl. Nano Mater. 2024, 7, 4814−4823

characteristic of $Ni(acac)_2$ and Se CVD created an ideal environment for the growth of CNTs, encapsulating the formed $NiSe_2$. As the reaction progresses, the carbon species generated through the decomposition of $Ni(acac)_2$ diffuse into the catalyst. The supersaturation of the catalyst then leads to the precipitation of carbon in the form of CNTs. $Ni(acac)_2$ hence serves as a single-source precursor, providing an ideal source for the formation of CNTs. Figure 1a depicts the XRD

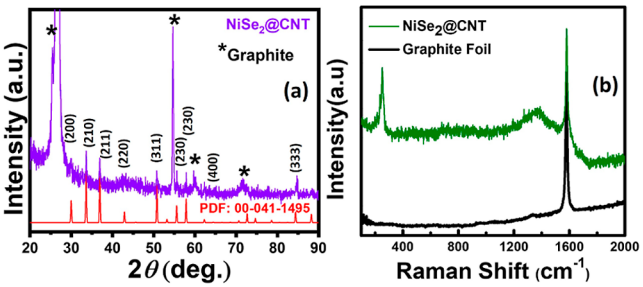

Figure 1. (a) PXRD and (b) Raman spectra of as-synthesized $NiSe_2$@CNT composite on graphite foil.

patterns of $NiSe_2$@CNT, which shows weak diffraction peaks from the sample that could be matched to the $NiSe_2$ standard diffraction pattern (PDF no. 00-041−1495). While the diffraction peaks suggested random orientation of the crystalline domains, some lattice planes such as (210) showed strong intensity, which was also observed in transmission electron microscopy (TEM) studies as explained below. The graphite peaks were mostly from the substrate. The $NiSe_2$@CNT sample was further analyzed using Raman spectroscopy, as shown in Figure 1b. $NiSe_2$ exhibited Raman peaks at 217 and 243 cm^{-1}, corresponding to the A_{1g} and T_{1g} modes, respectively.[30] Raman peaks at 1386 and 1580 cm^{-1} were attributed to the CNT. The "D-band" at 1386 cm^{-1} is most likely the result of disorder introduced into these nanostructures. The 1578 cm^{-1} peak was observed as a result of the Raman-active E_{2g}, which is comparable to graphite.[43] TEM was used to investigate the morphology of the $NiSe_2$@CNT composite. TEM analysis revealed the presence of CNTs throughout the sample as shown in Figure 2a. It also revealed that each CNT was filled with $NiSe_2$ wherein the diameters of the $NiSe_2$ filling ranged from 10 to 30 nm, as observed in different regions of the sample as well as between different batches. By examining numerous $NiSe_2$@CNT structures, it was revealed that the typical filling length of $NiSe_2$ is in the 300−500 nm range (Figure 2a). The high degree of crystallinity of the encapsulated $NiSe_2$ nanostructure was revealed by HRTEM images in Figure 2b, which showed lattice fringes in the $NiSe_2$ filling with a layer spacing of 0.268 nm. This specific layer spacing corresponds to the (210) lattice planes of $NiSe_2$, which had been previously identified through XRD analysis. This suggests that the average orientation of the $NiSe_2$ filling is at an angle of approximately 30° from the (210) lattice direction. In Figure 2c, the lattice fringes from the CNT walls could be seen by changing the focus to the CNT region, and a layer spacing of 0.34 nm was obtained from the CNT walls, indicating some degree of graphitization. This structural observation emphasizes the consistent presence of both the CNT and $NiSe_2$ components, indicating their stable coexistence. The lattice fringes from the CNT walls have been included as an inset of Figure 2c.

The chemical composition of the $NiSe_2$@CNT composite was further studied through XPS. Figure 3 depicts high-resolution Ni 2p, Se 3d, and C 1s spectra of the $NiSe_2$@CNT composite. Gaussian distributions were used to fit the high-resolution XPS spectra of these elements. The high-resolution Ni 2p spectrum (Figure 3a) can be deconvoluted into Ni^{2+} peaks at 857.2 eV (Ni $2p_{3/2}$) and 875.2 eV (Ni $2p_{1/2}$), multielectron excitation satellite peak at 863.4 eV, and shake peak at 877.5 eV (Ni $2p_{1/2}$). It should be noted here that the authors have previously reported this $NiSe_2$@CNT composite as electrocatalyst for oxygen evolution, and the XPS spectra for the current batch of samples matches with that reported previously.[30] The prominent peaks at 54.2 and 53.5 eV in the high-resolution Se 3d XPS spectrum shown in Figure 3b can be assigned to Se $3d_{3/2}$ and $3d_{5/2}$, respectively.[44] Furthermore, as a result of minor surface oxidation, there is a shoulder peak at 59.1 eV that can be assigned to the Se−O.[45] The high-resolution XPS spectra of C 1s (Figure 3c) reveals two peaks at 284.4 and 286.1 eV corresponding to the C−C and C−O bands, respectively.[46,47]

Electrochemical Biosensor Performance. In order to evaluate the electrochemical reactivity of the target DA molecule, CV and DPV measurements were carried out in a 0.1 M PBS solution. The method employs square wave potential pulses of constant height superimposed on a linearly increasing potential from the initial value to the final value. DPV, which has limited time resolution, is more sensitive than other electrochemical techniques as a full scan can take longer than seconds. Redox properties of DA make it more sensitive to detection by DPV because that method can eliminate non-Faradaic current. To investigate the oxidation and reduction behavior of DA at the modified $NiSe_2$@CNT electrode, DPV was performed in 0.1 M PBS for varied concentrations of DA ranging from 1 to 100 μM as shown in Figure 4a. It should be noted that at varied concentrations of DA ranging from 1 to 100 μM, the changes in currents are proportional, as shown in

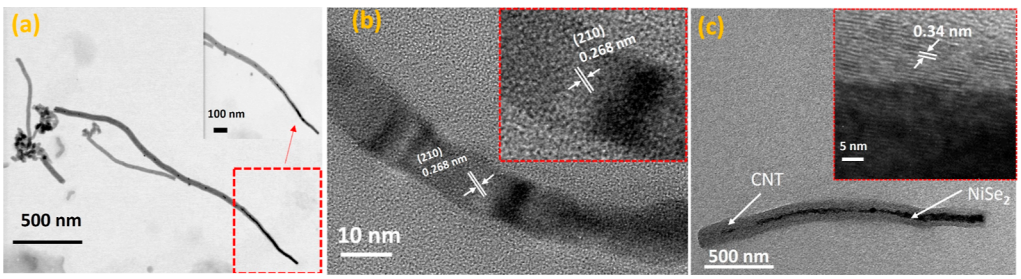

Figure 2. (a−c) TEM images of $NiSe_2$@CNTs. (b) Lattice fringes in the filling region corresponding to the presence of $NiSe_2$ crystalline domains. Inset shows magnified version of the lattice fringes. The inset in (c) shows a close-up of the CNT wall revealing graphitization.

https://doi.org/10.1021/acsanm.3c05422
ACS Appl. Nano Mater. 2024, 7, 4814−4823

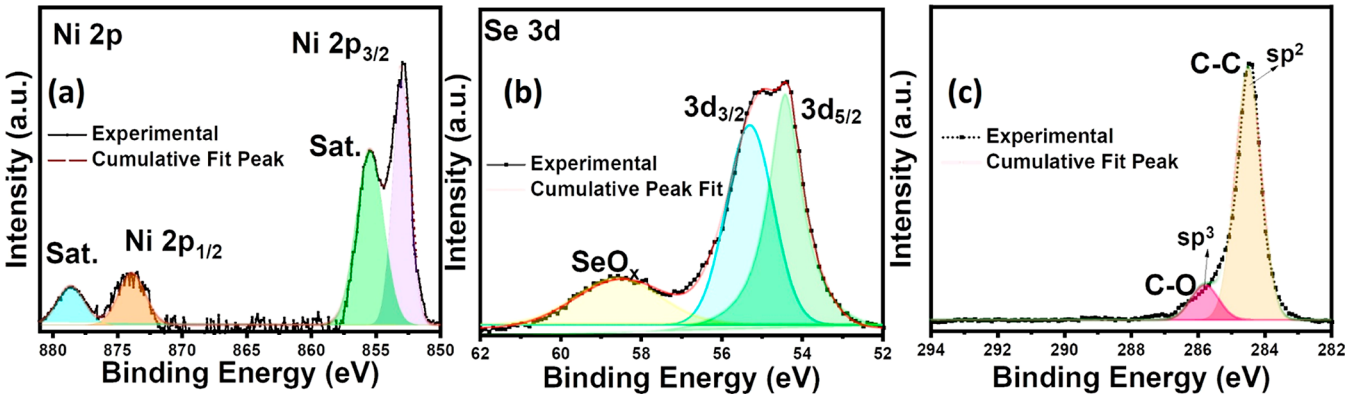

Figure 3. High-resolution XPS spectra of (a) Ni, (b) Se, and (c) C.[30]

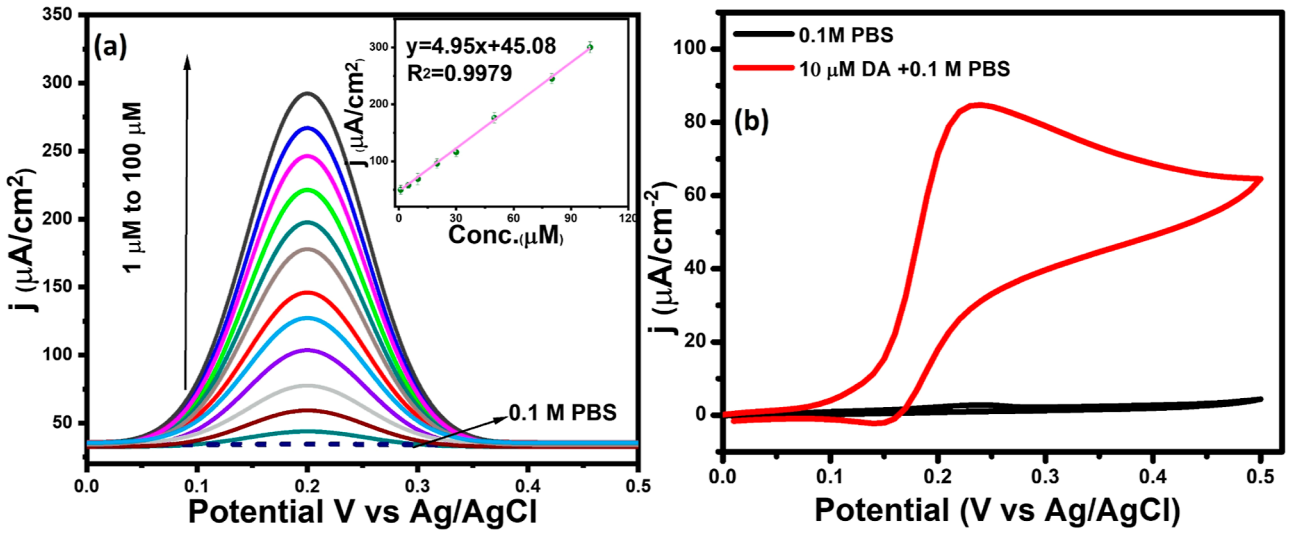

Figure 4. (a) DPV plots of $NiSe_2$@CNT in 0.1 M PBS buffer in the presence of increasing concentrations of DA. The inset shows corresponding calibration curves showing linear fit in the concentration range of 1−100 μM. (b) CV of the $NiSe_2$@CNT catalyst with 10 μM DA and without DA.

the inset of Figure 4a. The sensitivity of 4.95 μA μM^{-1} was estimated from the linear function

$$I_{pa}\ (\mu A) = 4.95 C_{DA}\ (\mu M) + 45.08 \quad (1)$$

with a correlation coefficient of $R^2 = 0.9979$, indicating that the $NiSe_2$@CNT electrode is highly sensitive toward detection of the DA molecule.

A CV experiment was used to study the reaction kinetics at the surface of the $NiSe_2$@CNT in the presence of 10 μM DA at scan speeds of 10 mV/s. As illustrated in Figure 4b, there is no apparent oxidation current across a wide range of potentials when the $NiSe_2$@CNT-modified electrode is tested in a PBS solution without DA. In contrast, after the addition of 10 μM DA, there was a considerable rise in the oxidation peak at 0.2 V, depicting the oxidation of dopamine to o-dopamine quinone (mechanism shown in Scheme 1a). The oxidation of DA at such a low potential validated the higher electrocatalytic activity of $NiSe_2$@CNT for DA oxidation.

To gain deeper insights into the electro-oxidation mechanism of DA on the surface of $NiSe_2$@CNT, an investigation was conducted to measure the oxidation peak current as a function of scan rate. Cyclic voltammograms were recorded in 10 μM DA solution at various scan rates, namely, 5, 10, 25, 50, and 75 mV s^{-1} (Figure S1). The oxidation peak potential (E_{pa}) showed a linear correlation with the log of the scan rate (ν) and could be expressed by the equation $E_{pa} = 0.057 \log \nu + 2.45$, with a high correlation coefficient ($R^2 = 0.9968$). In accordance with Laviron's theory,[48] the slope of this linear correlation is given by $2.303RT/\alpha n_\alpha F$, where α represents the electron transfer coefficient, n_α is the number of transferred electrons, F is the Faraday constant, R is the universal gas constant, and T is the temperature in Kelvin. The calculated value of αn_α was determined to be 1.04. Because the value of the transfer coefficient (α) is 0.5 for an irreversible process,[49−52] it could be concluded that the rate-limiting step closely resembles a two-electron transfer process, ($n_\alpha \sim 2$).

We have also conducted control experiments for DA sensing using separate electrodes coated with just $NiSe_2$ or CNT. The DPV and CV experiments revealed compelling results. While both CNT and NiSe-modified electrodes showed some activity for DA oxidation, a significant difference in the oxidation potential of DA was observed for CNT (0.24 V vs AglAgCl) compared with $NiSe_2$-based (0.2 V) electrodes. This suggests that $NiSe_2$ is a more efficient electrocatalyst for DA oxidation and also confirms that in the $NiSe_2$@CNT composite, Ni is the actual catalytic site. Ni-chalcogenides are known for their electrocatalytic activity owing to the facile electrochemical activation of the Ni site.[53−55] Moreover, as shown in Figure S2a,b, the current density of the $NiSe_2$@CNT composite

https://doi.org/10.1021/acsanm.3c05422
ACS Appl. Nano Mater. 2024, 7, 4814−4823

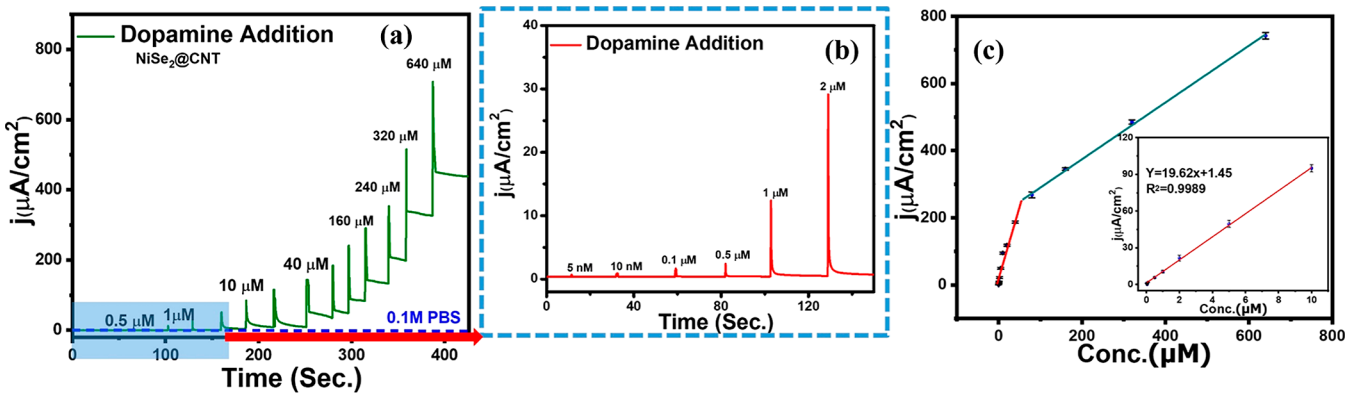

Figure 5. (a) Chronoamperometric measurements of the $NiSe_2$@CNT catalyst at 0.2 V potential vs Ag/AgCl with addition of a low to high concentration of DA. (b) Chronoamperometric measurements for a lower concentration range of DA addition. (c) Peak current vs concentration of DA at low and high DA concentrations. The inset shows the linear range from 5 nM to 10 μM.

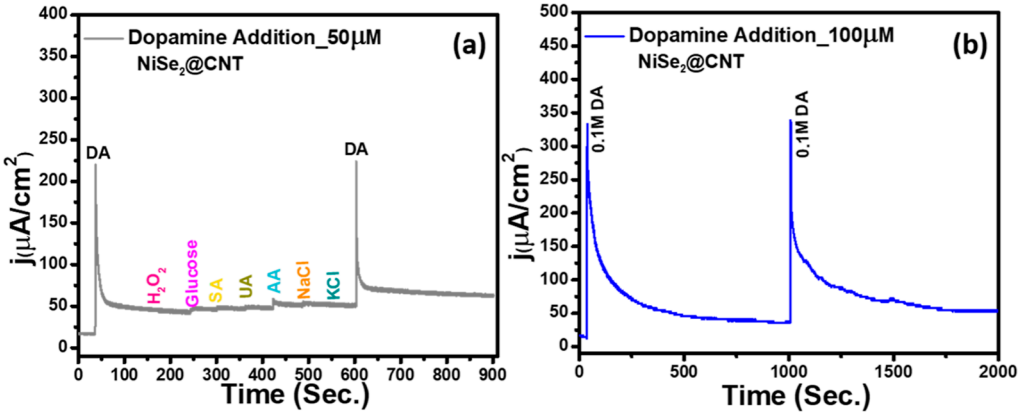

Figure 6. (a) Chronoamperometric response of DA oxidation on the $NiSe_2$@CNT electrode in 0.1 M PBS electrolyte with successive additions of 0.1 mM DA and other common interferents. (b) Chronoamperometric response at an applied potential of 0.20 V in 0.1 M PBS for long-term stability and reproducibility of the DA sensor.

demonstrated an approximately 2-fold increase compared to $NiSe_2$ alone and an impressive 6-fold increase compared to CNT. The control experiments, hence, suggest that while Ni (in $NiSe_2$) is the catalytic site for DA oxidation, encapsulating in within the CNT structure imparts favorable electrocatalytic performance for DA oxidation, making $NiSe_2$@CNT a superior electrocatalyst for selective DA sensing.

Furthermore, the CA measurement was used for DA detection, which is capable of obtaining lower detection limits because of its enhanced current sensitivity as well as its capacity to attenuate nonfaradic current. Consequently, the amperometric responses of the $NiSe_2$@CNT modified electrode in varied concentrations of DA were obtained at a 0.2 V applied potential. As shown in Figure 5a,b, with increasing DA concentrations, there was a linear increase in the faradic current. However, as shown by the linear fit of the amperometry data in Figure 5c, the increase in the oxidation current is proportional to the increase in the DA concentration. The anodic peak current as a function of DA concentration was plotted to create a calibration plot, as shown in Figure 5c, which shows a linear region in both low and high concentration ranges. The electrode's sensitivity was calculated to be 19.62 $\mu A\ \mu M^{-1}\ cm^{-2}$ based on the slope of the linear region in the low concentration range of 5 nM to 80 μM (inset of Figure 5c). Because carbon electrodes have been shown to be active for biomolecule oxidation, we have also performed chronoamperometric measurements of the bare graphite foil electrode (heated at 800 °C) at 0.2 V vs Ag/AgCl with addition of low to high concentrations of DA as shown in Figure S2c. The graphite foil showed very low oxidation current compared with the amperometric responses of the $NiSe_2$@CNT modified electrode. Furthermore, DPV studies were also performed on the bare graphite foil in 0.1 M PBS buffer in the presence and absence of concentrations of 100 μM DA to check the effect of the as-chosen graphite foil substrate (Figure S2d). As expected, the graphite foils did not show any oxidation peak in DPV studies and showed a very small anodic current in CA studies for the DA oxidation, which can be attributed to carbonization of the graphite foil at such a high temperature. This also confirmed that the observed activity for the composite electrode was because of the $NiSe_2$@CNT hybrid nanostructure. The combination of $NiSe_2$ and CNTs creates a synergistic effect where the unique properties of both materials complement each other. The $NiSe_2$ structure can facilitate catalytic electron transfer at the electrode−analyte interface, while CNTs provide a conductive platform for facile charge transfer within the electrode composite. When these two materials are integrated, they enhance the overall electrochemical reactivity, leading to an improved sensitivity and selectivity for DA sensing.

Selectivity is the most important attribute to consider when evaluating the actual applicability of the electrochemical

https://doi.org/10.1021/acsanm.3c05422
ACS Appl. Nano Mater. 2024, 7, 4814−4823

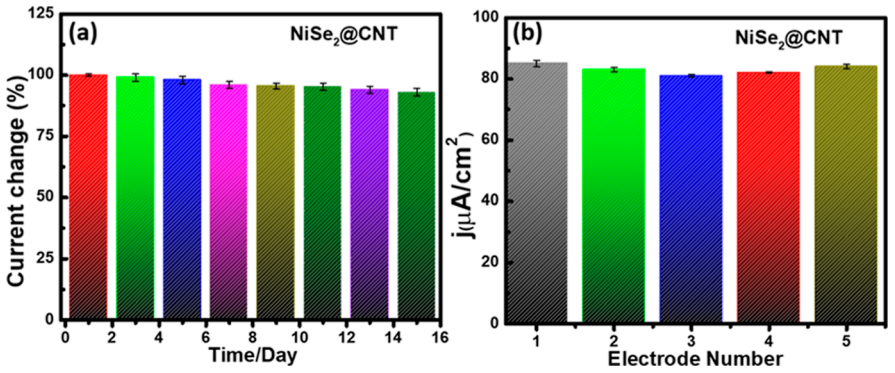

Figure 7. (a) DA sensors for 15 days show a reproducible current signal upon daily addition of 10 μM DA. (b) Reproducibility of the $NiSe_2$@CNT modified electrode for five different electrodes upon addition of 10 μM DA.

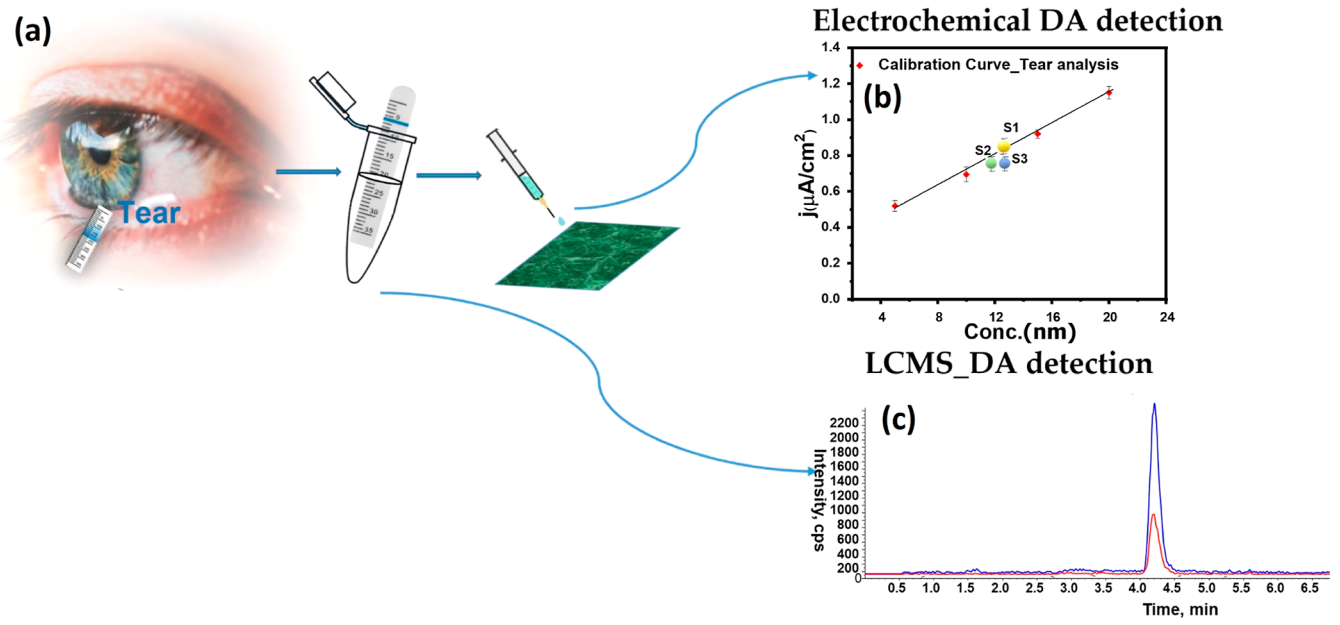

Figure 8. (a) Scheme illustrating detection of dopamine in human tears through catalytic conversion of dopamine-to-dopamine quinone. (b) Mean calibration curve of chronoamperometric measurements for DA detection from a human tear sample. (c) LCMS analysis of DA in human tear.

sensor. The interference investigation was carried out by assessing the efficacy of DA detection in the presence of several interferents such as AA, glucose, UA, KCl, H_2O_2, SA, and NaCl. As shown in Figure 6a, a chronoamperometric experiment was conducted in which the $NiSe_2$@CNT modified electrode was kept at an applied potential of 0.2 V versus Agl AgCl in a 0.1 M PBS electrolyte, while known concentrations (0.1 mM) of DA and other interfering compounds were added sequentially to the same electrolyte. The addition of 0.1 mM DA elicited strong current responses, whereas no significant current responses were observed when additional interferents were added. Additionally, the same concentration of DA was added at the end of the CA experiment to check the electrode's reproducibility after exposure to other chemical compounds, which demonstrated the same current response as the initial DA addition, indicating the electrode's high reproducibility. As a result, it was found that the $NiSe_2$@CNT catalyst was highly selective for DA oxidation at 0.2 V versus AglAgCl and had minimal interference from other analytes commonly present in physiological fluids.

The reproducibility of the $NiSe_2$@CNT electrode toward DA oxidation was further tested by introducing 0.1 mM DA in 0.1 M PBS and performing subsequent measurements. In Figure 6b, as 0.1 mM DA was added to the electrolyte at a constant applied potential of 0.2 V versus AglAgCl, there was a sharp increase in oxidation current, which gradually decreased over time as the added DA in the electrolyte was oxidized. After 1000 s, the same amount of DA solution was added to the solution, resulting in an almost similar increase in oxidation current. This study proved the electrode's repeatability and reusability toward DA oxidation. In Figure S3a, we conducted 100 cycles of DPV to evaluate sensitivity across multiple cycles of DA detection, and the outcomes were in alignment with our initial observations. Along with reproducibility, reusability of the sensor is another critical factor for practical applications. Hence, the CA technique was used to assess the functional stability of the as-prepared electrochemical DA sensor. A standard DA oxidation current was measured using the same electrode for 15 days under ambient conditions to assess the sensor's long-term stability, reproducibility, and reusability. As shown in Figure 7a, even after 15 days, the $NiSe_2$@CNT electrode maintained a 93% current response for DA sensing, demonstrating the outstanding durability of this electrode. Also 5 different batches of electrodes were prepared and tested to

https://doi.org/10.1021/acsanm.3c05422
ACS Appl. Nano Mater. 2024, 7, 4814−4823

test the reproducibility of the as-prepared electrode for the DA sensor (Figure 7b). The $NiSe_2$@CNT-based sensor had a relative standard deviation percentage (RSD percent) of less than 5% between different batches of the electrodes, demonstrating a high degree of repeatability in all measurements. Further, the CA technique was also used to assess the functional stability of the as-prepared electrochemical DA sensor. A standard DA oxidation current was measured using the same electrode for 7 days under ambient conditions to assess the sensor's long-term stability, reproducibility, and reusability. As shown in Figure S3b, the $NiSe_2$@CNT electrode sustained a current response of approximately 99% for DA sensing even after 7 days. This was confirmed through CV and the calibration curve of the CA test, highlighting the remarkable durability of the electrode. The electrode demonstrated a sensitivity of ∼19.57 $\mu A\ \mu M^{-1}$ after 7 days, further emphasizing its reliability and reproducibility for DA detection. In Figure S4, additional evidence of the compositional stability of the $NiSe_2$@CNT composite is presented, wherein, Raman spectroscopy and XPS analysis conducted before and after the electrochemical activity revealed no alterations in the surface composition of the composite.

Because DA is a critical neurochemical related to several ailments, its real-time detection in peripheral physiological fluids is of prime interest. Among these, designing noninvasive methods of detection will have significant impact. The $NiSe_2$@CNT-based electrode was used to measure DA levels in human tear samples without any pretreatment. Noninvasive tear sampling is a great alternative to blood or cerebrospinal fluid sampling for screening of peripheral biomarkers. Figure 8a shows a graphical representation to demonstrate the method of tears collection using Schirmer strips, extraction into analytes, and further analysis. Tear samples were collected from three individuals of varied age. The procedure typically involves placing the Schirmer strip at a specific location in the eye, often near the lower eyelid, allowing it to come into contact with the eye's surface. As tears are naturally produced, they get absorbed by the strip. The collected tears on the Schirmer strip can then be further analyzed for electrochemical DA detection. In accordance with the established protocol, the CA experiment was replicated, maintaining a constant applied potential of 0.2 V vs the AglAgCl electrode. A series of CA tests were conducted by using three tear samples collected from different individuals (Figure S5). The current response for DA addition was calibrated with a standard solution of 5 nM DA in PBS solution. This standard DA solution was injected into the electrolyte at fixed intervals twice before injecting the tear solution and twice after. The calibration line was constructed by plotting the current response of the standard DA solution. Figure 8b represents the relationship between the recorded current response and the concentration of DA in the standard solutions, which shows a linear plot as expected. The concentration of DA in the tear samples was estimated from this calibration plot by mapping the observed current response to the specific concentration. The DA levels in the collected tear samples varied between 4 and 7 nM, which is in good agreement with typical DA levels found in healthy individuals.[56]

An additional step was taken to confirm and validate the DA concentration in the tear samples. This verification was achieved by measuring the DA level in the collected tear samples using liquid chromatography-tandem mass spectrometry (LC−MS/MS) with MRM, a highly precise analytical technique commonly employed for the identification and quantification of various compounds. Figures S6 and 8c show the cumulative results of the LC−MS/MS analysis. Briefly, two ion-pairs (the optimized MS/MS parameters shown in Table S1) were used for DA quantitation and confirmation, shown as blue and red peaks in the chromatogram. The method was validated, and the spike recovery fell within the range of 95−105%, affirming the accuracy and reliability of the detection process. Further application of the LC−MS method to tear samples confirmed the presence of DA in the collected tears. Moreover, quantification of the LC−MS data showed that the level of DA in the collected tear samples was ∼7 nM, similar to the amount detected through electrochemical measurements. The LC−MS data hence further confirmed the high level of accuracy of the electrochemical sensor.

Table S2 provides a summary of the performance of various Ni-based electrochemical DA sensors, as reported in the literature, including a comparison of the linear range, detection limit, and sensitivity. Among them, $NiSe_2$@CNT reported in this study has a wide linear range, a low determination limit, and a high sensitivity for DA sensing. CNT-metal chalcogenide nanostructures offer a plethora of advantages over other composites when used as an electrochemical sensor. The exceptional electrochemical sensing performance can be explained as follows: (i) the significant advantage benefits from the hybridization of CNT and metal chalcogenides, where the high electrical conductivity and surface area of the CNT counterpart may contribute to high current; (ii) redox centers imparted by the transition metal and chalcogenide sites are extremely advantageous for electrocatalytic sensing of DA; (iii) the existence of a redox center within this nanostructure leads to a wide linear range, higher selectivity, and sensitivity toward analyte detection; (iv) lower electronegativity of the chalcogenide anion enhances electron density around the catalytically active transition-metal center, which optimizes the electrochemical activation steps.

CONCLUSIONS

Freestanding CNT-encapsulated nickel selenide nanocomposites were produced on a graphite foil and used to detect DA by using various electrochemical methods. The fabricated electrochemical sensor demonstrated superior sensitivity, stability, and repeatability for DA detection. More importantly, the as-prepared sensor could be used to detect DA levels in collected tear samples with a high level of accuracy. The synergetic electrochemical performance of $NiSe_2$ and CNTs, as well as the quick charge transferability between the electrochemical sites and the electrode, can be attributed to such enhanced selectivity and superior performance as a nonenzymatic biosensor.

ASSOCIATED CONTENT

Supporting Information

The Supporting Information is available free of charge at https://pubs.acs.org/doi/10.1021/acsanm.3c05422.

Effect of the CV scan rate in PBS; comparison of DPV and CV plots of $NiSe_2$@CNT, $NiSe_2$, and CNT; chronoamperometric measurements of a bare graphite foil electrode; DPV plots of a bare graphite foil; peak current vs concentration of DA at a low DA concentration; Raman spectra and XPS spectra before and after DA oxidation; CA at a constant potential of 0.2

https://doi.org/10.1021/acsanm.3c05422
ACS Appl. Nano Mater. 2024, 7, 4814−4823

V with the addition of DA and the collected tear sample: LC−MS chromatograms (PDF)

AUTHOR INFORMATION

Corresponding Author

Manashi Nath − *Department of Chemistry, Missouri University of Science and Technology, Rolla, Missouri 65409, United States;* orcid.org/0000-0002-5058-5313; Email: nathm@mst.edu

Authors

Harish Singh − *Department of Chemistry, Missouri University of Science and Technology, Rolla, Missouri 65409, United States*

Jiandong Wu − *Department of Chemistry, Missouri University of Science and Technology, Rolla, Missouri 65409, United States*

Kurt A. L. Lagemann − *Department of Chemistry, Missouri University of Science and Technology, Rolla, Missouri 65409, United States*

Complete contact information is available at: https://pubs.acs.org/10.1021/acsanm.3c05422

Notes

The authors declare no competing financial interest.

ACKNOWLEDGMENTS

The authors would like to acknowledge partial financial support from NSF CAS-2155175 and Materials research center (MRC), Missouri S&T for equipment usage. We would also like to acknowledge Dr. Nuran Ercal, (Professor, Department of chemistry, Missouri S&T) for assistance with LCMS data collection.

REFERENCES

(1) Latif, S.; Jahangeer, M.; Maknoon Razia, D.; Ashiq, M.; Ghaffar, A.; Akram, M.; El Allam, A.; Bouyahya, A.; Garipova, L.; Ali Shariati, M.; Thiruvengadam, M.; Azam Ansari, M. Dopamine in Parkinson's Disease. *Clin. Chim. Acta* **2021**, *522*, 114−126.

(2) Klein, M. O.; Battagello, D. S.; Cardoso, A. R.; Hauser, D. N.; Bittencourt, J. C.; Correa, R. G. Dopamine: Functions, Signaling, and Association with Neurological Diseases. *Cell. Mol. Neurobiol.* **2019**, *39* (1), 31−59.

(3) Di Chiara, G.; Bassareo, V.; Fenu, S.; De Luca, M. A.; Spina, L.; Cadoni, C.; Acquas, E.; Carboni, E.; Valentini, V.; Lecca, D. Dopamine and Drug Addiction: The Nucleus Accumbens Shell Connection. *Neuropharmacology* **2004**, *47* (Suppl 1), 227−241.

(4) Skotland, T.; Ljones, T. Direct Spectrophotometric Detection of Ascorbate Free Radical Formed by Dopamine β-Monooxygenase and by Ascorbate Oxidase. *Biochim. Biophys. Acta, Gen. Subj.* **1980**, *630* (1), 30−35.

(5) Parsons, L. H.; Kerr, T. M.; Weiss, F. Simple Microbore High-Performance Liquid Chromatographic Method for the Determination of Dopamine and Cocaine from a Single In Vivo Brain Microdialysis Sample. *J. Chromatogr. B: Biomed. Sci. Appl.* **1998**, *709* (1), 35−45.

(6) Li, L.; Liu, H.; Shen, Y.; Zhang, J.; Zhu, J. J. Electrogenerated Chemiluminescence of Au Nanoclusters for the Detection of Dopamine. *Anal. Chem.* **2011**, *83* (3), 661−665.

(7) Umapathi, S.; Masud, J.; Coleman, H.; Nath, M. Electrochemical Sensor Based on CuSe for Determination of Dopamine. *Microchim. Acta* **2020**, *187* (8), 440.

(8) Singh, H.; Bernabe, J.; Chern, J.; Nath, M. Copper Selenide as Multifunctional Non-Enzymatic Glucose and Dopamine Sensor. *J. Mater. Res.* **2021**, *36* (7), 1413−1424.

(9) Reddy, S.; Kumara Swamy, B. E.; Jayadevappa, H. CuO Nanoparticle Sensor for the Electrochemical Determination of Dopamine. *Electrochim. Acta* **2012**, *61*, 78−86.

(10) Sriram, B.; Kogularasu, S.; Wang, S. F.; Sheu, J. K. Deep Eutectic Solvent-Mediated Synthesis of Spinel Zinc Chromite Nanoparticles: A Simple Label-Free Electrochemical Sensor for Dopamine and Ascorbic Acid. *ACS Appl. Nano Mater.* **2023**, *6*, 17593−17602.

(11) Maseed, H.; Reddy Yenugu, V. M.; Devarakonda, S. S. B.; Petnikota, S.; Gajulapalli, M.; Srikanth, V. V. S. S. Peroxidase-like Fe_3O_4 Nanoparticle/Few-Layered Graphene Composite for Electrochemical Detection of Dopamine, Ascorbic Acid, and Uric Acid. *ACS Appl. Nano Mater.* **2023**, *6*, 18531−18538.

(12) Shen, C. H.; Chang, Y. N.; Chen, Y. L.; Kung, C. W. Sulfonate-Grafted Metal-Organic Framework−A Porous Alternative to Nafion for Electrochemical Sensors. *ACS Mater. Lett.* **2023**, *5* (7), 1938−1943.

(13) Xi, X.; Tang, W.; Wu, D.; Shen, C.; Ji, W.; Li, J.; Su, Y.; Guo, X.; Liu, R.; Yan, F. All-Carbon Solution-Gated Transistor with Low Operating Voltages for Highly Selective and Stable Dopamine Sensing. *ACS Sens.* **2023**, *8* (3), 1211−1219.

(14) Figueiredo-Filho, L. C. S.; Silva, T. A.; Vicentini, F. C.; Fatibello-Filho, O. Simultaneous Voltammetric Determination of Dopamine and Epinephrine in Human Body Fluid Samples Using a Glassy Carbon Electrode Modified with Nickel Oxide Nanoparticles and Carbon Nanotubes within a Dihexadecylphosphate Film. *Analyst* **2014**, *139* (11), 2842−2849.

(15) Umapathi, S.; Singh, H.; Masud, J.; Nath, M. Nanostructured Copper Selenide as an Ultrasensitive and Selective Non-Enzymatic Glucose Sensor. *Mater. Adv.* **2021**, *2*, 927−932.

(16) Jahani, S.; Beitollahi, H. Selective Detection of Dopamine in the Presence of Uric Acid Using NiO Nanoparticles Decorated on Graphene Nanosheets Modified Screen-Printed Electrodes. *Electroanalysis* **2016**, *28* (9), 2022−2028.

(17) Ma, F.; Yang, B.; Zhao, Z.; Zhao, Y.; Pan, R.; Wang, D.; Kong, Y.; Chen, Y.; Huang, G.; Kong, J.; Mei, Y. Sonication-Triggered Rolling of Janus Porous Nanomembranes for Electrochemical Sensing of Dopamine and Ascorbic Acid. *ACS Appl. Nano Mater.* **2020**, *3* (10), 10032−10039.

(18) Shen, Y.; Sheng, Q.; Zheng, J. A High-Performance Electrochemical Dopamine Sensor Based on a Platinum-Nickel Bimetallic Decorated Poly(Dopamine)-Functionalized Reduced Graphene Oxide Nanocomposite. *Anal. Methods* **2017**, *9* (31), 4566−4573.

(19) Golrokh Amin, B.; De Silva, U.; Masud, J.; Nath, M. Ultrasensitive and Highly Selective Ni_3Te_2 as a Nonenzymatic Glucose Sensor at Extremely Low Working Potential. *ACS Omega* **2019**, *4* (6), 11152−11162.

(20) Nath, M.; Singh, H.; Saxena, A. Progress of Transition Metal Chalcogenides as Efficient Electrocatalysts for Energy Conversion. *Curr. Opin. Electrochem.* **2022**, *34*, 100993.

(21) Singh, H.; Prendergast, D.; Nath, M. Modulation of Electrocatalytic Activity by Tuning Anion Electronegativity: Case Study with Copper Chalcogenides. *J. Phys.: Energy* **2023**, *5*, 045016.

(22) Xia, X.; Shen, X.; Du, Y.; Ye, W.; Wang, C. Study on Glutathione's Inhibition to Dopamine Polymerization and Its Application in Dopamine Determination in Alkaline Environment Based on Silver Selenide/Molybdenum Selenide/Glassy Carbon Electrode. *Sens. Actuators, B* **2016**, *237*, 685−692.

(23) Savariraj, A. D.; Vinoth, V.; Mangalaraja, R. V.; Arun, T.; Contreras, D.; Akbari-Fakhrabadi, A.; Valdés, H.; Banat, F. Microwave-Assisted Synthesis of Localized Surface Plasmon Resonance Enhanced Bismuth Selenide (Bi_2Se_3) Layers for Non-Enzymatic Glucose Sensing. *J. Electroanal. Chem.* **2020**, *856*, 113629.

(24) Baye, A. F.; Appiah-Ntiamoah, R.; Amalraj, J.; Reddy, K. K.; Kim, H. Graphene Oxide Interlayered Ga-Doped $FeSe_2$ Nanorod: A Robust Nanocomposite with Ideal Electronic Structure for Electrochemical Dopamine Detection. *Electrochim. Acta* **2020**, *363*, 137245.

(25) Yang, X.; Zhang, J.; Wang, Z.; Wang, H.; Zhi, C.; Yu, D. Y. W.; Rogach, A. L. Carbon-Supported Nickel Selenide Hollow Nanowires as Advanced Anode Materials for Sodium-Ion Batteries. *Small* **2018**, *14* (7), 1−9.
(26) Saxena, A.; Liyanage, W.; Masud, J.; Kapila, S.; Nath, M. Selective Electroreduction of CO_2 to Carbon-Rich Products with a Simple Binary Copper Selenide Electrocatalyst. *J. Mater. Chem. A* **2021**, *9* (11), 7150−7161.
(27) Saxena, A.; Liyanage, W.; Kapila, S.; Nath, M. Nickel Selenide as an Efficient Electrocatalyst for Selective Reduction of Carbon Dioxide to Carbon-Rich Products. *Catal. Sci. Technol.* **2022**, *12*, 4727−4739.
(28) Saxena, A.; Singh, H.; Nath, M. Cobalt Telluride Electrocatalyst for Selective Electroreduction of CO_2 to Value-Added Chemicals. *Mater. Renew. Sustain. Energy* **2022**, *11*, 115−129.
(29) Nath, M.; De Silva, U.; Singh, H.; Perkins, M.; Liyanage, W. P. R.; Umapathi, S.; Chakravarty, S.; Masud, J. Cobalt Telluride: A Highly Efficient Trifunctional Electrocatalyst for Water Splitting and Oxygen Reduction. *ACS Appl. Energy Mater.* **2021**, *4* (8), 8158−8174.
(30) Singh, H.; Liyanage, W. P. R.; Nath, M. Carbon Nanotube Encapsulated Metal Selenide Nanostructures for Efficient Electrocatalytic Oxygen Evolution Reaction. *Chem. Commun.* **2022**, *58* (60), 8360−8363.
(31) Masud, J.; Liyanage, W. P. R.; Cao, X.; Saxena, A.; Nath, M. Copper Selenides as High-Efficiency Electrocatalysts for Oxygen Evolution Reaction. *ACS Appl. Energy Mater.* **2018**, *1* (8), 4075−4083.
(32) Zhai, L.; Benedict Lo, T. W.; Xu, Z. L.; Potter, J.; Mo, J.; Guo, X.; Tang, C. C.; Edman Tsang, S. C.; Lau, S. P. In Situ Phase Transformation on Nickel-Based Selenides for Enhanced Hydrogen Evolution Reaction in Alkaline Medium. *ACS Energy Lett.* **2020**, *5* (8), 2483−2491.
(33) Du, L.; Du, W.; Ren, H.; Wang, N.; Yao, Z.; Shi, X.; Zhang, B.; Zai, J.; Qian, X. Honeycomb-like Metallic Nickel Selenide Nanosheet Arrays as Binder-Free Electrodes for High-Performance Hybrid Asymmetric Supercapacitors. *J. Mater. Chem. A* **2017**, *5* (43), 22527−22535.
(34) Singh, H.; Nath, M.; Hines, M. M. Development of High-Performance Electrode Materials for Supercapacitor Application through Combinatorial Electrodeposition. *ECS Meet. Abstr.* **2022**, *MA2022-01* (3), 492.
(35) Wu, H.; Wang, Y.; Zhang, L.; Chen, Z.; Wang, C.; Fan, S. Comparison of Two Nickel Selenides Materials with Different Morphologies as Counter Electrodes in Dye-Sensitized Solar Cells. *J. Alloys Compd.* **2018**, *745*, 222−227.
(36) Wang, W.; Cui, Q.; Sun, D.; Yang, Q.; Xu, J.; Liao, W.; Zuo, X.; Tang, H.; Li, G.; Jin, S. Enhanced Electrocatalytic Performance in Dye-Sensitized Solar Cell via Coupling $CoSe_2$@N-Doped Carbon and Carbon Nanotubes. *J. Mater. Chem. C* **2021**, *9* (22), 7046−7056.
(37) Sivasakthi, S.; Imran, H.; Karuppasamy, G.; Sagadevan, S.; Mohammad, F.; Dharuman, V. Green Synthesis of Porous Carbon Nanocubes Accumulated Microspheres for the Simultaneous Non-Enzymatic Sensing of Uric Acid and Dopamine in the Presence of Ascorbic Acid. *Synth. Met.* **2020**, *270*, 116598.
(38) Foroughi, F.; Rahsepar, M.; Kim, H. A Highly Sensitive and Selective Biosensor Based on Nitrogen-Doped Graphene for Non-Enzymatic Detection of Uric Acid and Dopamine at Biological PH Value. *J. Electroanal. Chem.* **2018**, *827*, 34−41.
(39) Anshori, I.; Nuraviana Rizalputri, L.; Rona Althof, R.; Sean Surjadi, S.; Harimurti, S.; Gumilar, G.; Yuliarto, B.; Handayani, M. Functionalized Multi-Walled Carbon Nanotube/Silver Nanoparticle (f-MWCNT/AgNP) Nanocomposites as Non-Enzymatic Electrochemical Biosensors for Dopamine Detection. *Nanocomposites* **2021**, *7* (1), 97−108.
(40) Mercante, L. A.; Pavinatto, A.; Iwaki, L. E. O.; Scagion, V. P.; Zucolotto, V.; Oliveira, O. N.; Mattoso, L. H. C.; Correa, D. S. Electrospun Polyamide 6/Poly(Allylamine Hydrochloride) Nanofibers Functionalized with Carbon Nanotubes for Electrochemical Detection of Dopamine. *ACS Appl. Mater. Interfaces* **2015**, *7* (8), 4784−4790.
(41) Singh, H.; Marley-Hines, M.; Chakravarty, S.; Nath, M. Multi-Walled Carbon Nanotube Supported Manganese Selenide as Highly Active Bifunctional OER and ORR Electrocatalyst. *J. Mater. Chem. A* **2022**, *10*, 6772−6784.
(42) Li, J. P. H.; Zhou, X.; Pang, Y.; Zhu, L.; Vovk, E. I.; Cong, L.; Van Bavel, A. P.; Li, S.; Yang, Y. Understanding of Binding Energy Calibration in XPS of Lanthanum Oxide by In Situ Treatment. *Phys. Chem. Chem. Phys.* **2019**, *21* (40), 22351−22358.
(43) Zhang, H. B.; Lin, G. D.; Zhou, Z. H.; Dong, X.; Chen, T. Raman Spectra of MWCNTs and MWCNT-Based H2-Adsorbing System. *Carbon* **2002**, *40* (13), 2429−2436.
(44) Chen, H.; Fan, M.; Li, C.; Tian, G.; Lv, C.; Chen, D.; Shu, K.; Jiang, J. One-Pot Synthesis of Hollow NiSe-CoSe Nanoparticles with Improved Performance for Hybrid Supercapacitors. *J. Power Sources* **2016**, *329*, 314−322.
(45) Tang, C.; Zhao, Z. L.; Chen, J.; Li, B.; Chen, L.; Li, C. M. Se-$Ni(OH)_2$-Shelled Vertically Oriented NiSe Nanowires as a Superior Electrocatalyst toward Urea Oxidation Reaction of Fuel Cells. *Electrochim. Acta* **2017**, *248*, 243−249.
(46) Gu, Y.; Fan, L. Q.; Huang, J. L.; Geng, C. L.; Lin, J. M.; Huang, M. L.; Huang, Y. F.; Wu, J. H. N-Doped Reduced Graphene Oxide Decorated $NiSe_2$ Nanoparticles for High-Performance Asymmetric Supercapacitors. *J. Power Sources* **2019**, *425*, 60−68.
(47) Yadav, K. K.; Singh, H.; Rana, S.; Sunaina; Sammi, H.; Nishanthi, S. T.; Wadhwa, R.; Khan, N.; Jha, M. Utilization of Waste Coir Fibre Architecture to Synthesize Porous Graphene Oxide and their Derivatives: An Efficient Energy Storage Material. *J. Clean. Prod.* **2020**, *276*, 124240.
(48) Laviron, E. Adsorption, Autoinhibition and Autocatalysis in Polarography and in Linear Potential Sweep Voltammetry. *J. Electroanal. Chem. Interfacial Electrochem.* **1974**, *52* (3), 355−393.
(49) Rountree, E. S.; Mccarthy, B. D.; Eisenhart, T. T.; Dempsey, J. L. Evaluation of Homogeneous Electrocatalysts by Cyclic Voltammetry. *Inorg. Chem.* **2014**, *53* (19), 9983−10002.
(50) Zheng, J.; Yan, Y.; Xu, B. Correcting the Hydrogen Diffusion Limitation in Rotating Disk Electrode Measurements of Hydrogen Evolution Reaction Kinetics. *J. Electrochem. Soc.* **2015**, *162* (14), 1470−1481.
(51) Moghaddam, M.; Sepp, S.; Wiberg, C.; Bertei, A.; Rucci, A.; Peljo, P. Thermodynamics, Charge Transfer and Practical Considerations of Solid Boosters in Redox Flow Batteries. *Molecules* **2021**, *26* (8), 2111.
(52) Deng, W.; Zhang, P.; Seger, B.; Gong, J. Unraveling the Rate-Limiting Step of Two-Electron Transfer Electrochemical Reduction of Carbon Dioxide. *Nat. Commun.* **2022**, *13* (1), 803.
(53) Sivanantham, A.; Shanmugam, S. Nickel Selenide Supported on Nickel Foam as an Efficient and Durable Non-Precious Electrocatalyst for the Alkaline Water Electrolysis. *Appl. Catal., B* **2017**, *203*, 485−493.
(54) Swesi, A. T.; Masud, J.; Liyanage, W. P. R.; Umapathi, S.; Bohannan, E.; Medvedeva, J.; Nath, M. Textured $NiSe_2$ Film: Bifunctional Electrocatalyst for Full Water Splitting at Remarkably Low Overpotential with High Energy Efficiency. *Sci. Rep.* **2017**, *7* (1), 2401.
(55) De Silva, U.; See, J.; Liyanage, W. P. R.; Masud, J.; Wu, J.; Yang, W.; Chen, W.-T.; Prendergast, D.; Nath, M. Understanding the Structural Evolution of a Nickel Chalcogenide Electrocatalyst Surface for Water Oxidation. *Energy Fuels* **2021**, *35* (5), 4387−4403.
(56) Sharma, N. S.; Acharya, S. K.; Nair, A. P.; Matalia, J.; Shetty, R.; Ghosh, A.; Sethu, S. Dopamine Levels in Human Tear Fluid. *Indian J. Ophthalmol.* **2019**, *67* (1), 38−41.

https://doi.org/10.1021/acsanm.3c05422
ACS Appl. Nano Mater. 2024, 7, 4814−4823